Journal of Himalayan Earth Sciences Volume, No., 2026 pp. 1-10

Groundwater Potential Delineation Using Electrical Resistivity Tomography (ERT) in the Kohat Region, Khyber Pakhtunkhwa, Pakistan

Beenish Ali[1], Jabir Nazir[2]*, and Ihtisham Ullah[3]

[1]Department of Geology, Bacha Khan University, Charsadda, Pakistan
[2]Mineral Exploration Development Operations (MEDO), FWO, Islamabad, Pakistan
[3]Abdul Wali Khan University, Mardan, Pakistan
**Corresponding author: jabirgeop@gmail.com*

Submitted Date:23/04/2026, Acceptance Date: 10/08/2026, Publication Date:---------

Abstract

This study delineates groundwater-potential zones in the Kohat region of Khyber Pakhtunkhwa, Pakistan, using Electrical Resistivity Tomography (ERT) integrated with existing well information and GIS-based groundwater-potential mapping. Four north–south ERT profiles were acquired using 34 electrodes at 20 m spacing, giving a maximum profile length of 660 m. The data were processed and inverted to obtain two-dimensional resistivity sections, then the four profiles were integrated to construct a three-dimensional resistivity model in Voxler. Inverted resistivity range from approximately 5 to 750 Ω·m and show marked lateral and vertical heterogeneity. Low-to-moderate resistivity zones (approximately 10–110 Ω·m) occur mainly within the shallow 0–30 m interval and are interpreted as groundwater-potential zones, with responses consistent with unconsolidated to semi-consolidated materials and increased moisture content. Intermediate resistivity zones at approximately 30–80 m are interpreted as weathered or fractured material in selected parts of the profiles, whereas high-resistivity zones generally correspond to competent, relatively dry or low-permeability formations. The 3D model indicates spatially discontinuous conductive and structurally controlled zones, with comparatively favorable conditions in the northern and central parts of the surveyed area and less favorable conditions toward the west. Comparison with the published GIS/MIF groundwater-potential model and nearby well information indicates broad agreement between shallow ERT responses and reported groundwater occurrence. A candidate exploratory drilling target is retained near 560 m along Line 01; however, the ERT interpretation should be verified by lithological logging, water-level measurements, and pumping tests before groundwater development. The study demonstrates the value of integrating surface-based groundwater mapping with subsurface geophysical imaging for local-scale groundwater exploration in the Kohat region.

***Keywords*:** Electrical Resistivity Tomography; groundwater potential; resistivity inversion; 3D resistivity model; Kohat Basin; hydrogeophysics

1. Introduction

Groundwater is an important and persistent source of freshwater, but its availability is spatially heterogeneous and strongly controlled by geological, climatic, and hydrological conditions (Konikow and Kendy, 2005). In Pakistan, groundwater is particularly important for agriculture, domestic supply, and local economic activity. Increasing water demand, climate variability, population growth, urbanization, and declining reliability of some surface-water sources have increased pressure on groundwater resources (Khair et al., 2012; Faheem et al., 2023; Nazir et al., 2025).

Groundwater scarcity is particularly relevant in the semi-arid parts of Khyber Pakhtunkhwa, including the southern districts of the province. Previous regional assessments have demonstrated spatial variations in groundwater potential across Kohat and neighboring areas, but GIS- and remote-sensing-based approaches primarily characterize surface and near-surface controlling factors and provide limited direct information on subsurface geometry (Faheem et al., 2023; Nazir et al., 2025). Local-scale groundwater exploration therefore benefits from methods capable of imaging vertical and lateral changes in subsurface electrical properties.

Electrical Resistivity Tomography (ERT) is widely used for near-surface hydrogeophysical investigations because contrasts in electrical resistivity can reflect changes in lithology, porosity, moisture, clay content, and groundwater saturation (Reynolds, 2011). The method is particularly useful for identifying conductive zones, weathered or fractured intervals, and resistive competent formations. Importantly, resistivity responses are non-unique; therefore, groundwater interpretation should be constrained by geological information and independent hydrogeological observations wherever possible.

The Kohat Basin contains a thick sedimentary succession ranging from Jurassic to Quaternary age. Major formations include the Jurassic, Datta, Samana Suk, Chichali, Lumshiwal, and Kawagarh formations; Paleogene units including Hangu, Lockhart, Patala, Nammal, Sakesar, and Kohat formations; and younger continental deposits including the Murree, Kamlial, Chinji, Nagri, Dhok Pathan, and Soan formations (Meissner et al., 1974; Ahmad et al., 2024). Interbedded limestone, sandstone, shale, gypsum, and unconsolidated deposits provide contrasting hydrogeological properties. Fractured carbonate rocks may provide secondary porosity and pathways for groundwater movement (Khan et al., 2022), while structural features and lithological heterogeneity influence recharge, storage, and groundwater flow (Khan et al., 2018; Faheem et al., 2023).

The present study was undertaken in District Kohat, located at approximately 33.58° N and 71.43° E, at an elevation of about 490 m above mean sea level (Fig. 1). The study area occurs within semi-arid to sub-humid subtropical climatic conditions, where geology, rainfall, drainage, and soil influence groundwater recharge (Ahmad et al., 2025). Published groundwater-potential mapping indicates predominantly moderate potential in much of the district, with lower recharge potential in hilly and elevated areas where steep slopes can reduce infiltration (Nazir et al., 2025).

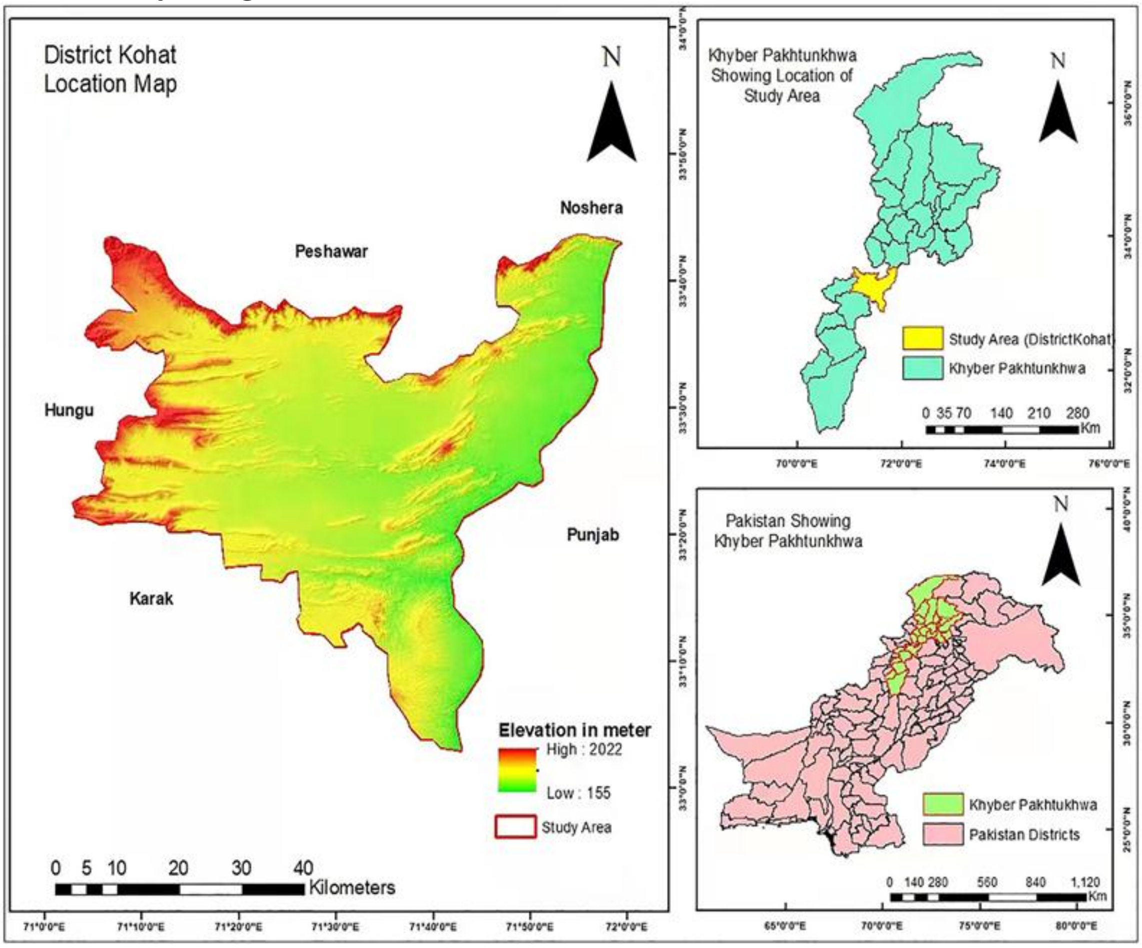

Fig. 1. Study-area location in District Kohat and regional geographic context.

The objective of this study is to delineate subsurface groundwater-potential zones using four ERT profiles, characterize their lateral and vertical continuity, integrate the profiles through 3D resistivity modelling, and compare the geophysical interpretation with available well information and published GIS/MIF groundwater-potential mapping. The study also identifies candidate locations for further hydrogeological investigation while explicitly recognizing the limitations of resistivity-based groundwater interpretation.

2. Geological and Hydrogeological Setting

The Kohat Basin forms part of the Himalayan foreland system and comprises sedimentary rocks deposited during the evolution of the Tethyan margin and subsequent Himalayan deformation (Meissner et al., 1974; Ahmad et al., 2024). The stratigraphic succession contains contrasting permeable and relatively impermeable units. Limestone and sandstone may provide primary or secondary storage where porosity and fracturing are sufficiently developed, whereas shale, clay-rich materials, gypsum, and competent unfractured rock can restrict groundwater movement. Consequently, groundwater occurrence in the study area is expected to depend on the combined effects of lithology, weathering, fracturing, topography, drainage, and recharge.

Published work on the Kohat region indicates that groundwater potential varies spatially and that lineaments and geological structures can influence groundwater flow and storage (Faheem et al., 2023; Khan et al., 2018; Nazir et al., 2025). The present ERT survey is therefore interpreted as a subsurface complement to existing surface-based groundwater-potential information rather than as an independent measure of groundwater quantity or sustainable yield.

3. Materials and Methods

3.1 ERT survey design and acquisition

Four ERT profiles (L-01 to L-04) were acquired in a north–south orientation across previously identified groundwater-potential target areas. An ABEM Terrameter SAS 4000 resistivity system with stainless-steel electrodes, cables, and a control unit was used. Each profile comprised 34 electrodes with 20 m electrode spacing, resulting in a maximum profile length of 660 m (Table 1, Fig. 2). The dipole–dipole configuration was selected because of its sensitivity to lateral resistivity variations and its suitability for imaging structurally controlled subsurface features. The dipole–dipole array generally provides good lateral resolution but can have a lower signal-to-noise ratio than some alternative arrays; this characteristic was considered during data-quality assessment (Reynolds, 2011).

Table 1: Summary of the ERT survey configuration and processing information.

Parameter	Description
Number of profiles	4 (L-01 to L-04)
Profile orientation	North–south
Electrodes per profile	34
Electrode spacing	20 m
Maximum profile length	660 m
Array	Dipole–dipole
Instrument	ABEM Terrameter SAS 4000
Inversion software	AGI Earth-Imager
3D visualization/interpolation	Voxler
Reported RMS error	<10% overall; individual displayed sections vary

3.2 Apparent resistivity and inversion

Electrical current was injected into the subsurface through current electrodes, and the resulting potential difference was measured between potential electrodes. For the dipole–dipole configuration, the apparent resistivity is expressed in Equations (1 and 2).

$$\rho_a = K\,\Delta V / I \qquad \text{……… (1)}$$

$$K = \pi\, a\, n(n + 1)(n + 2) \qquad \text{……… (2)}$$

where ρ_a is apparent resistivity, K is the geometric factor, a is electrode spacing, n is the dipole-separation factor, ΔV is the measured potential difference, and I is the injected current. The measured apparent-resistivity data were processed and inverted using AGI Earth-Imager to obtain subsurface resistivity distributions. Data quality was evaluated using the root-mean-square (RMS) misfit; the manuscript reports an RMS error below 10% as the general quality criterion. Because the inverted resistivity model is non-unique, geological and hydrogeological interpretation was based on the spatial continuity and magnitude of resistivity anomalies together with published geological and well information.

3.3 Three-dimensional resistivity modelling

The four inverted ERT profiles were integrated in Voxler to visualize the three-dimensional distribution of resistivity and to assess the spatial continuity of conductive and resistive zones. The resulting 3D representation is an interpolation between the measured profiles and should therefore be regarded as a spatial visualization of the ERT-derived resistivity field rather than a direct three-dimensional measurement. Fracture-related interpretations were made where discontinuous resistivity contrasts occurred in positions that were spatially consistent with the interpreted structural framework.

3.4 Groundwater interpretation and validation

Resistivity values were interpreted using relative contrasts rather than a universal resistivity threshold. Low to moderate resistivity may reflect increased moisture or groundwater saturation, but conductive responses can also result from clay-rich materials or other conductive lithologies. Conversely, high resistivity commonly indicates compact or relatively dry material but does not by itself prove the absence of groundwater. Groundwater-potential zones were therefore identified where resistivity, geometry, depth, and continuity were compatible with the available geological and hydrogeological information.

Validation was performed by comparing the ERT-derived shallow groundwater-potential zones with the published MIF groundwater-potential model and nearby well information reported by Faheem et al. (2023). The published well information indicates groundwater occurrence within approximately 0–35 m, while the ERT interpretation identifies a broadly comparable shallow interval of approximately 0–30 m. The original manuscript reports an 85.7% agreement between the datasets; however, the calculation procedure and validation criteria are not documented. Therefore, the present study does not use 85.7% as a quantitative validation statistic. Instead, the comparison is treated as a broad correspondence between the shallow ERT groundwater-potential interval (approximately 0- 30 m) and the reported groundwater occurrence interval (approximately 035 m). A quantitative agreement metric should only be reported after the underlying classification method, comparison units, and calculation are explicitly documented.

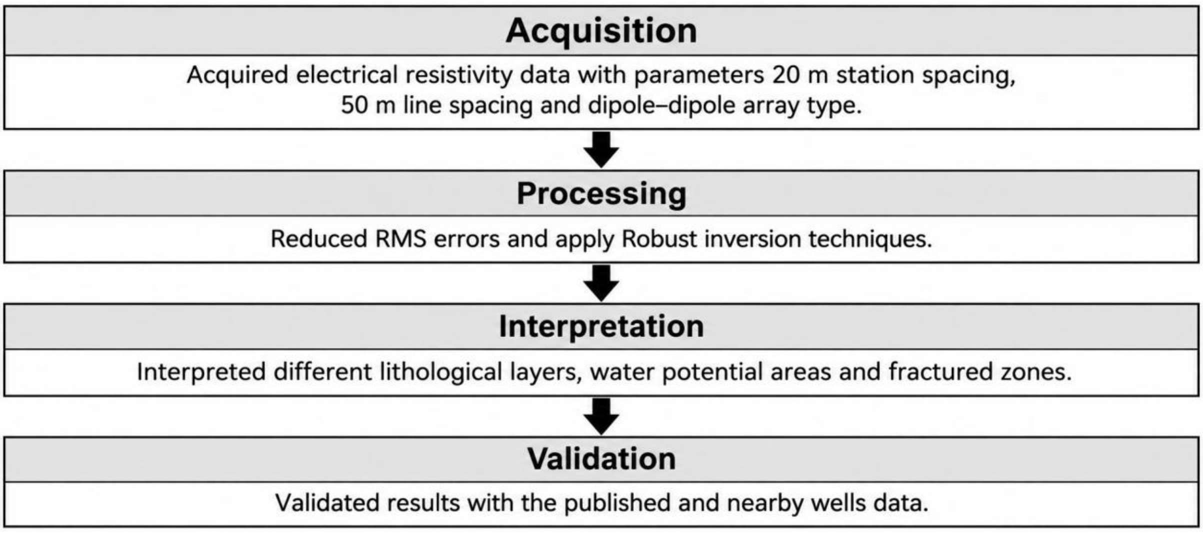

Fig. 2. Workflow for ERT acquisition, processing, inversion, interpretation, 3D modelling, and validation.

4. Results and Discussion

4.1 Inverted resistivity characteristics of Lines L-01 and L-02

The inverted sections of L-01 and L-02 show substantial lateral and vertical variation, with resistivity ranging from approximately 5 to 750 Ω·m. On L-01, the shallow 0–30 m interval is dominated by low to moderate resistivity (approximately 10–110 Ω·m), consistent with unconsolidated to semi-consolidated materials containing variable moisture. A relatively continuous moderate-resistivity zone of approximately 100–250 Ω·m occurs between about X = 120–320 m and extends locally to 60–80 m depth. This zone is interpreted as comparatively less conductive material with limited evidence for strong groundwater saturation (Fig. 3). A high-resistivity anomaly exceeding approximately 500 Ω·m occurs around X = 440–500 m and is interpreted as a competent, relatively dry or low-permeability body.

L-02 shows weaker shallow groundwater-potential signatures than L-01. The central to eastern part of the profile, approximately X = 300–600 m, is dominated by moderate to high resistivity, suggesting comparatively less conductive and potentially drier or more competent material. Localized resistive bodies exceeding 500 Ω·m are consistent with hard or compact formations. The interpretation indicates that groundwater potential is spatially heterogeneous rather than continuous along the entire profile.

4.2 Inverted resistivity characteristics of Lines L-03 and L-04

L-03 and L-04 display a broadly comparable three-zone geoelectrical pattern. The near-surface interval, approximately 0–30 m, contains variable resistivity values of about 5–100 Ω·m (Fig. 4). These conductive to moderately conductive responses are compatible with mixtures of clay, silt, and partially saturated sediments. At intermediate depths of approximately 30–80 m, resistivity is commonly around 50–100 Ω·m in parts of the sections. These zones may represent weathered or fractured material, but their interpretation as productive aquifer horizons remains conditional because similar resistivity values can also occur in clay-rich formations.

A particularly notable conductive zone occurs on L-04 between approximately X = 450–600 m, where resistivity falls within roughly 5–50 Ω·m. This feature is interpreted as a groundwater-potential zone only where its geometry and geological context support increased saturation; clay-rich material remains an alternative explanation. At greater depths, resistivity of approximately 150–750 Ω·m become more dominant, especially toward the right-hand portions of the sections, and are interpreted as comparatively competent or consolidated formations with lower expected permeability.

4.3 Comparative interpretation of groundwater-potential zones

Table 2 summarizes the principal interpreted resistivity domains and their hydrogeological significance. The interpretation is deliberately expressed in terms of groundwater potential rather than confirmed aquifer occurrence because ERT does not directly measure groundwater yield.

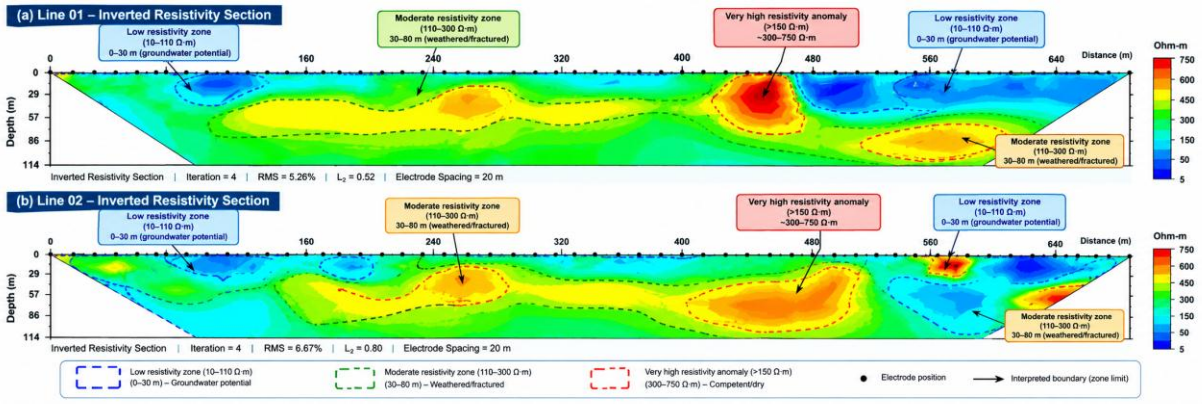

Fig. 3. Inverted north–south ERT sections for (a) L-01 and (b) L-02. The sections show lateral and vertical resistivity variations and the interpreted groundwater-potential interval.

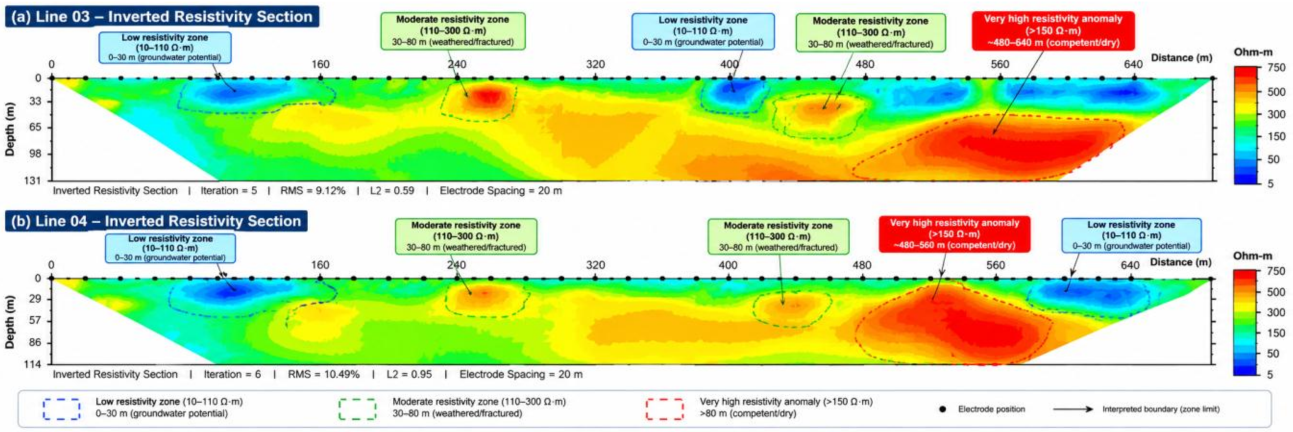

Fig. 4. Inverted north–south ERT sections for (a) L-03 and (b) L-04, showing conductive shallow/intermediate zones and deeper resistive formations.

Table 2: Principal interpreted resistivity domains and their hydrogeological significance.

Profile	Depth/position	Resistivity	Interpretation	Groundwater
L-01	0–30 m; shallow zone	10–110 Ω·m	Moist unconsolidated/semi-consolidated material	Potential shallow groundwater zone
	X≈120–320 m; 60–80 m	100–250 Ω·m	Moderately resistive material	Limited evidence for strong saturation
	X≈440–500 m	>500 Ω·m	Competent/highly resistive body	Likely low permeability; not a primary target
L-02	X≈300–600 m	Moderate–high	Partly saturated to relatively dry/competent material	Generally, less favorable than conductive zones
L-03	0–30 m	5–100 Ω·m	Variable moist/clayey/silty sediments	Potential groundwater zone; clay is an alternative explanation
L-04	X≈450–600 m	5–50 Ω·m	Strong conductive anomaly	Potential saturated zone; requires verification
L-03/ L-04	>80 m	150–750 Ω·m	Competent/consolidated formations	Generally limited primary groundwater potential

4.4 Three-dimensional resistivity model

The 3D model provides a spatial view of resistivity variations between the four N–S profiles. Conductive and resistive domains are not uniformly distributed, indicating substantial lateral heterogeneity. The model highlights two broad structural or discontinuity zones, one toward the northern part and another toward the southern part of the surveyed area (Fig. 5). These features may provide preferential pathways for groundwater movement where they correspond to open, interconnected fractures. However, the 3D model is interpolated from four 2D profiles, so apparent continuity between profiles should not be treated as direct evidence of a continuous fracture network without additional data.

The northern and central sectors show comparatively more favorable combinations of shallow conductive responses and structural discontinuities, whereas the western sector is dominated more strongly by resistive material. This spatial pattern is consistent with the general concept that groundwater potential depends on the coexistence of storage material, permeability pathways, and recharge conditions rather than on resistivity magnitude alone.

4.5 Correlation with GIS/MIF mapping and well information

Faheem et al. (2023) used a multi-influencing-factor (MIF) approach and well information to map groundwater potential across Kohat District.

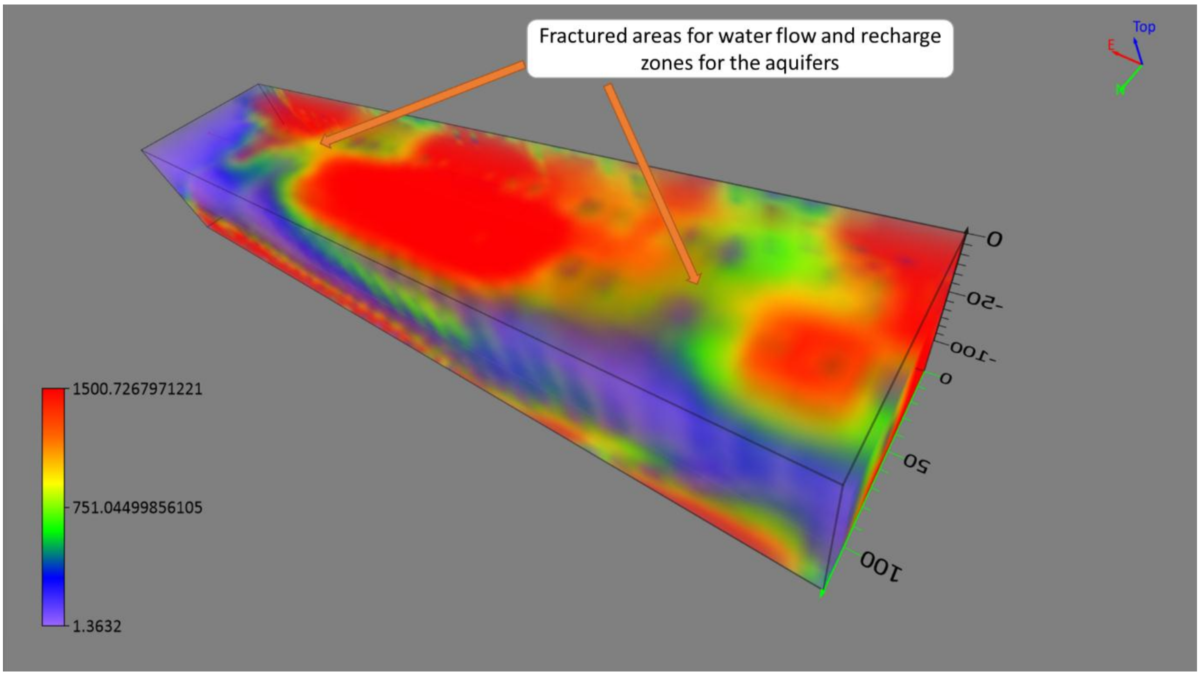

Fig. 5. Three-dimensional visualization of the interpolated ERT resistivity field and interpreted discontinuity/fracture-related zones.

That approach provides valuable regional and surface-related information but does not directly resolve the vertical distribution of subsurface resistivity. The present ERT results complement the MIF model by providing two-dimensional subsurface imaging and a 3D visualization of the resistivity field.

The published well information indicates groundwater occurrence at approximately 0–35 m, while the present ERT interpretation identifies a broadly comparable shallow groundwater-potential interval of approximately 0–30 m (Fig. 6). The original manuscript reported 85.7% agreement between the two datasets; however, the calculation procedure is not documented.

Accordingly, this study does not treat 85.7% as a validated quantitative accuracy measure. The comparison is limited to the broad correspondence between the ERT-derived shallow groundwater-potential interval (approximately 0–30 m) and the published groundwater occurrence interval (approximately 0–35 m). The two datasets therefore provide supporting evidence for the shallow interpretation, but they do not establish a quantitative prediction accuracy or groundwater yield. The comparison therefore supports the consistency of the shallow ERT interpretation but does not constitute a direct measurement of aquifer yield or groundwater quality.

4.6 Candidate borehole target and implications

Based on the existing interpretation, the manuscript identifies a candidate drilling position near X = 560 m on L-01. At this location, the interpreted shallow resistivity pattern is considered potentially favorable for groundwater exploration. Because the available text does not provide a sufficiently explicit layer boundary at exactly X = 560 m, the target should be described as a priority exploratory location rather than a confirmed productive well site.

The previously stated drilling depth of approximately 25 m should also be treated as a preliminary target depth. The manuscript elsewhere identifies potentially fractured or weathered zones at approximately 30–80 m depth. These intervals should be reconciled against the actual L-01 section before a final drilling depth is specified. A practical recommendation is therefore to use the ERT model to define the target interval and allow final borehole depth to be determined from drilling, lithological logging, water strikes, and subsequent hydraulic testing.

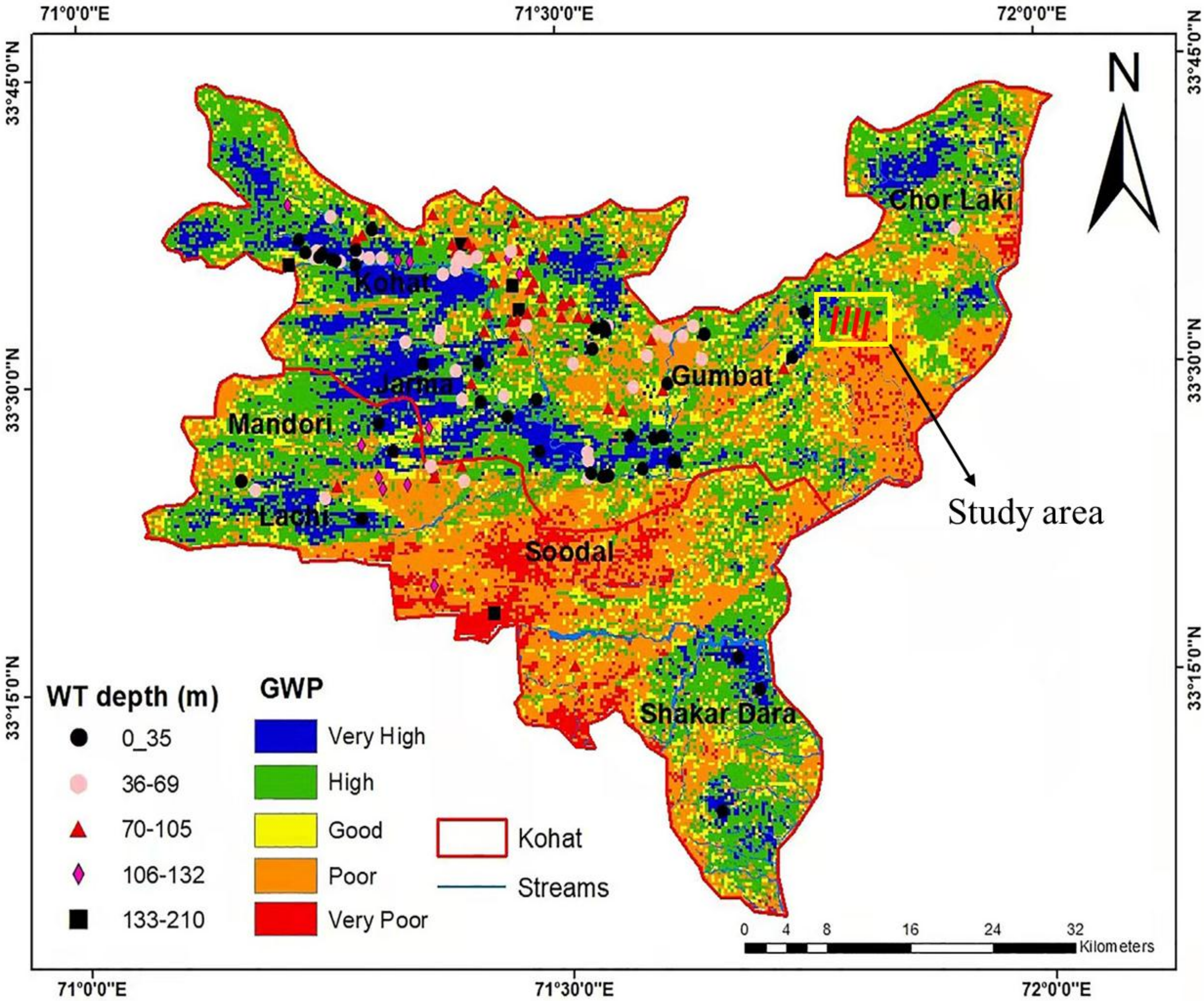

Fig. 6. Comparison of ERT-derived groundwater-potential zones with the published MIF groundwater-potential model and well information reported by Faheem et al. (2023).

4.7 Limitations and recommendations for verification

- ERT resistivity is non-unique; low resistivity may result from groundwater saturation, clay, salinity, or combinations of these factors.
- The 3D resistivity representation is interpolated between four 2D profiles and therefore has lower certainty away from the measured lines.
- The available well comparison provides depth-based validation but does not establish hydraulic conductivity, transmissivity, storativity, groundwater quality, or sustainable yield.
- The previously reported 85.7% agreement should not be presented as a quantitative validation statistic unless a reproducible calculation and clearly defined validation criterion are provided. In the present manuscript, validation is therefore expressed as qualitative depth-interval correspondence.
- The candidate L-01 target near X = 560 m should be verified through exploratory drilling, lithological logging, static water-level measurement, and pumping testing before development.
- Future surveys should consider additional cross-lines or alternative electrode arrays where feasible to improve structural interpretation and reduce ambiguity.

5. Conclusions

Four north–south ERT profiles in the Kohat region reveal pronounced lateral and vertical variations in subsurface resistivity, ranging from approximately 5 to 750 Ω·m. The results indicate a heterogeneous subsurface composed of shallow unconsolidated/semi-consolidated materials, locally weathered or fractured intervals, and deeper comparatively resistive formations.

Low to moderate resistivity responses, particularly within approximately

0–30 m depth, represent the principal groundwater-potential zones identified by the survey. These interpretations are supported by the broad correspondence between the ERT results and published well information, which reports groundwater occurrence within approximately 0–35 m.

The 3D resistivity model indicates spatially variable conductive and resistive domains and suggests that structural discontinuities may influence groundwater movement. The northern and central parts of the surveyed area show comparatively favorable combinations of conductive shallow material and structural features, whereas more resistive conditions dominate parts of the western sector.

An exploratory drilling target near X = 560 m along L-01 is retained as a candidate location. However, ERT alone cannot demonstrate sustainable yield or confirm an aquifer. The target depth should be finalized only after reconciling the interpreted resistivity boundaries at X = 560 m and should be verified by drilling, lithological logging, water-level measurements, and pumping tests.

Overall, the study demonstrates that ERT can provide useful local-scale subsurface information when integrated with geological, well, and GIS-based groundwater-potential evidence. The integrated approach can improve groundwater-target selection while reducing the risk of over-interpreting resistivity anomalies as confirmed groundwater resources.

Author Contributions

Jabir Nazir and Beenish Ali developed the main concept and contributed to ERT data acquisition, processing, and interpretation, including software and technical support. Ihtisham Ullah assisted with geophysical fieldwork and provided physiographic information for the study area.

Acknowledgements

The authors would like to express their sincere gratitude to Bacha Khan University Charsadda, for providing the necessary facilities and support to conduct this research. Special thanks are extended to the field team for their valuable assistance during the acquisition of the Electrical Resistivity Tomography (ERT) data.

Funding

The authors received no financial support for the research and publication of this article.

References

Ahmad, S., Kroon, D., Reijmer, J. J. G., Khan, S., Hersi, O. S., & Wadood, B. (2024). Paleogene carbonate ramp development in the Kohat Basin of northwestern Pakistan. *Australian Journal of Earth Sciences, 71*(2), 277–306. https://doi.org/10.1080/08120099.2023.2279062

Ahmad, S., Rigby, S., Kroon, D., Khan, S., & Haneef, M. (2011). Integrated Paleogene sequence stratigraphy of the Kohat Basin, northwest Pakistan. *Proceedings of the SPE-PAPG Annual Technical Conference 2011*, 81–92.

Ahmad, W., Liu, L., Guo, Z., Khalil, Y. S., Islam, N. U., & Islam, F. (2025). Lithological classification using ZY1-02D hyperspectral data by means of machine learning and deep learning methods in the Kohat–Pothohar Plateau, Khyber Pakhtunkhwa, Pakistan. *Remote Sensing*, *17*(8), 1356.

Faheem, H., Khattak, Z., Islam, F., Ali, R., Khan, R., Khan, I., & Tag Eldin, E. (2023). Groundwater potential zone mapping using geographic information systems and multi-influencing factors: A case study of the Kohat District, Khyber Pakhtunkhwa. *Frontiers in Earth Science*, *11*, 1097484.

Khair, S. M., Mushtaq, S., Culas, R. J., & Hafeez, M. (2012). Groundwater markets under water scarcity and declining watertable conditions: The upland Balochistan Region of Pakistan. *Agricultural Systems*, *107*, 21–32.

Khan, E., Naseem, A. A., Khan, S., Wadood, B., Rehman, F., Saleem, M., Mehmood, M., Ahmad, W., Ahmed, Z., & Azeem, T. (2022). Facies analysis, sequence stratigraphy and diagenetic studies of the Jurassic carbonates of the Kohat Basin, Northwest Pakistan:

Reservoir implications. *Acta Geologica Sinica (English Edition)*, *96*(5), 1673–1692. https://doi.org/10.1111/1755-6724.14938

Khan, M., Sayem, A. S. M., & Shah, M. (2018). Numerical groundwater flow modeling of Kohat basin: An example from Himalayan fold and thrust belt Pakistan. *MAUSAM*, *69*(2), 263–276. https://doi.org/10.54302/mausam.v69i2.305

Konikow, L. F., & Kendy, E. (2005). Groundwater depletion: A global problem. *Hydrogeology Journal*, *13*(1), 317–320. https://doi.org/10.1007/s10040-004-0411-8

Meissner, C. R., Jr., Master, J. M., Rashid, M. A., & Hussain, M. (1974). *Stratigraphy of the Kohat Quadrangle, Pakistan* (U.S. Geological Survey Professional Paper 716-D). U.S. Government Printing Office. https://doi.org/10.3133/pp716D

Nazir, J., Ali, M., Sarwar, A., Khan, S., Rehman, K., Fahim, B., & Iqbal, B. (2025). Delineation and validation of GIS-based groundwater potential zones under arid to semi-arid environment using multi-influence-factors approach. *Geology, Ecology, and Landscapes*, *9*(4), 1194–1210. https://doi.org/10.1080/24749508.2024.2392382

Reynolds, J. M. (2011). An Introduction to Applied and Environmental Geophysics (2nd ed.). Wiley-Blackwell.